Separation of Wear-Out Failure Modes of IGBT Modules in Grid-Connected Inverter Systems

Ui-Min Choi, *Member, IEEE*, and Frede Blaabjerg, *Fellow, IEEE*

***Abstract*—Wear-out condition monitoring of IGBT modules with failure mode separation gives some benefits. First, it allows proactive maintenance plans. Further, depending on the failure mode, different proactive control strategies can be applied to inverters in order to improve the reliability and availability of power electronic systems. This paper proposes a new method for the separation of two representative wear-out failure modes of wire-bonded IGBT modules in a grid-connected inverter in real time. The proposed method requires just two preliminary *I–V* characterizations of IGBT modules. Further, only one monitoring parameter is used, and thus, it is cost-effective compared with using one more monitoring parameter in order to separate failure modes. Experimental results verify the validity and feasibility of the proposed method.**

***Index Terms*—Condition monitoring, inverter, IGBT module, reliability, wear-out failure.**

I. Introduction

POWER inverters are one of the most reliability-critical parts in power electronic systems such as photovoltaic (PV) systems and wind-power generation systems [1]. For example, in [2], the unscheduled maintenance events and costs by the subsystems have been investigated based on field experiences between 2001 and 2006 in a large utility-scale PV generation plant. The PV inverter covers 37% of unscheduled maintenance events and make up 59% of unscheduled maintenance costs. In the case of wind turbine systems, around 350 wind turbines from multiple manufacturers have been investigated [3]. In total, 35 000 downtime events have been considered to determine the distribution of failure rates and downtimes between the subassemblies. It shows that the power electronic frequency converters cause 13% of the failures and 18.4% of the downtime of the monitored wind turbines. It can be seen from the earlier results that the inverter systems are one of the important parts in respect to the reliability in the overall PV and wind power generation systems and also to reduce the cost of operation.

The power inverters consist of various components such as power devices, gate drivers, capacitors, PCBs, and also inductors. Among them, the power devices are taking a great portion of main failure sources of inverters, and thus, they are key components in respect to the reliability of overall power electronic systems [4]–[6].

Manuscript received April 25, 2017; revised July 24, 2017; accepted August 31, 2017. Date of publication September 7, 2017; date of current version March 5, 2018. Recommended for publication by Associate Editor Wenping Cao. *(Corresponding author: Ui-Min Choi.)*

U.-M. Choi is with the Department of Electronic and IT Media Engineering, Seoul National University of Science and Technology, Seoul, Korea (e-mail: uch@et.aau.d).

F. Blaabjerg is with the Department of Energy Technology, Aalborg University, Aalborg 9220, Denmark (e-mail: fbl@et.aau.dk).

Color versions of one or more of the figures in this paper are available online at http://ieeexplore.ieee.org.

Digital Object Identifier 10.1109/TPEL.2017.2750328

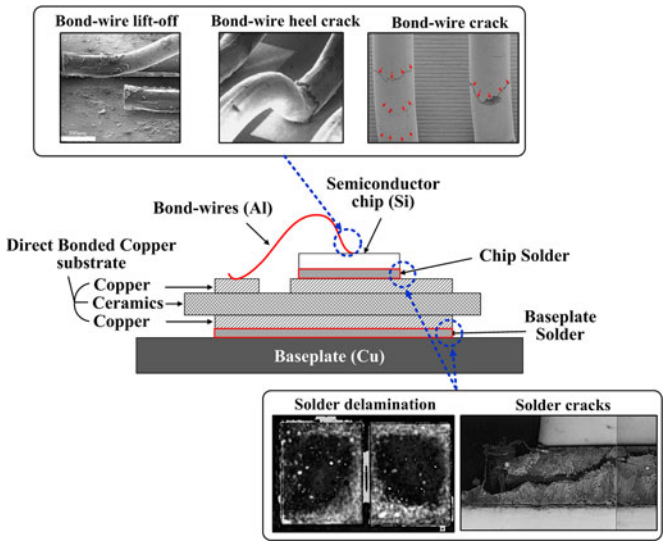

Fig. 1. Structure of a standard IGBT module and dominant package-related wear-out failure mechanisms [11].

An IGBT is one of the most widely used of their kind for various applications in the power range from several hundred watts to several megawatts [7].

In practical applications, an IGBT is used in a form of package-like discrete devices and modules for several purposes [7]. Typically, there are two types of IGBT modules: press-pack and wire-bonded IGBT modules, and between them, the wire-bonded IGBT modules are still widely used in various power electronic systems due to the cost aspect [8], [9].

In wire-bonded IGBT modules, there are mainly two types of package-related wear-out failure modes. Bond-wire fatigue is one of the common failure mechanisms in a standard power IGBT module [10], as illustrated in Fig. 1 [11]. The other dominant failure mechanism is solder joint fatigue between chip and direct bonded copper (DBC) substrate and between DBC substrate and base plate [10]. Both failure modes occur due to the large coefficient of thermal expansion (CTE) mismatch of materials, which compose IGBT modules under temperature variation due to the converter load variation, periodical commutation of the power switching devices, and also the ambient temperature change. The bond-wire fatigue increase the ohmic resistance and it appears as an increase in the on-state collector-emitter voltage (V_{CE_ON}) of transistors. The failure of

a single or small number of bond-wires alters the current distribution in power devices and accelerates the wear-out failure of the remaining bond-wires. Finally, it leads to catastrophic failures or open-circuit failure of power devices. In the case of solder joint fatigue, the thermal impedance of the IGBT module increases. Consequently, the junction temperature of the power devices may increase and thus $V_{\text{CE\_ON}}$ is changed, as it is a temperature-sensitive electrical parameter (TSEP) [12]. The thermal impedance increase could accelerate other failure modes like bond-wire fatigue. Furthermore, the increased junction temperature could induce hot spots and thermal runaway in the affected areas of the module [13]. As mentioned earlier, $V_{\text{CE\_ON}}$ is varied when both failure modes occur, and therefore, it is widely used for the condition monitoring of IGBT modules in respect to both bond-wire and solder joint fatigues [14]–[17].

However, it is worth to note that other types of failures such as failure in cooling systems also cause the increase of junction temperature, and thus, it should be clarified first if the increase of junction temperature is due to other factors or not when the solder joint fatigue is determined by the junction temperature increase.

A real-time wear-out condition monitoring of IGBT modules with the determination of failure modes can provide information for performing proactive control scheme such as load management and thermal control. Depending on the failure mechanism, different control strategies can be applied to inverters. For example, fault-tolerant control methods can be applied when wear-out failure occurs in bond-wires [6], [18]–[21] and active thermal control strategies can be used when the degradation in solder joint occurs [22]–[25] in order to reduce the highest temperature of the failed device in order to improve the reliability of the power electronic systems by extending the lifetime of inverters. Furthermore, it also allows proactive maintenance plans.

As mentioned earlier, $V_{\text{CE\_ON}}$ can be used for the monitoring of both failure modes. However, the $V_{\text{CE\_ON}}$ variation indicates two failure modes at the same time. In order to use $V_{\text{CE\_ON}}$ for the monitoring of both failure modes, it is needed to eliminate the influence from one failure mode on the monitoring of the other failure mode. For example, $V_{\text{CE\_ON}}$ can be used for the monitoring of the bond-wire fatigue and the junction temperature (T_j) estimation for the monitoring of the solder joint fatigue. However, if bond-wire fatigue occurs, the measured $V_{\text{CE\_ON}}$ increases, and it results in an increase in the estimated junction temperature. On the other hand, if the solder joint fatigue occurs, it also leads to an increase of $V_{\text{CE\_ON}}$. Therefore, an *I–V* characterization needs to be performed again in order to determine $V_{\text{CE\_ON}}$ increase either due to bond-wire fatigue or due to solder joint fatigue [26]. However, in real systems, the inverters have to be stopped and IGBT modules have to be detached from the inverters for *I–V* re-characterization of IGBT modules. This process is very inconvenient and time consuming. Other additional monitoring parameters can be used for junction temperature estimation in order to monitor the solder joint fatigue [27], [28], but it is not cost effective because an extra circuit for measuring an additional parameter is required.

This paper proposes a new method for monitoring the wear-out status of IGBT modules in the grid-connected inverter with the separation of two representative failure modes by monitoring the $V_{\text{CE\_ON}}$ values at two points with two initial *I–V* characterizations of the IGBT module.

Experimental results verify the validity and feasibility of the proposed method.

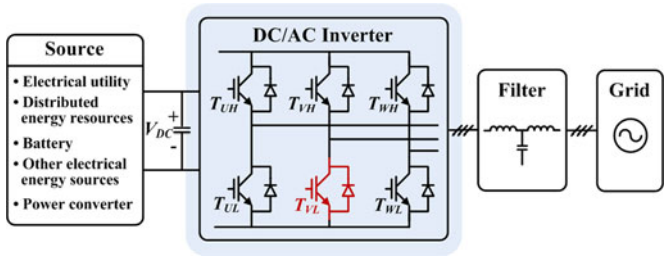

Fig. 2. Configuration of a grid-connected inverter system.

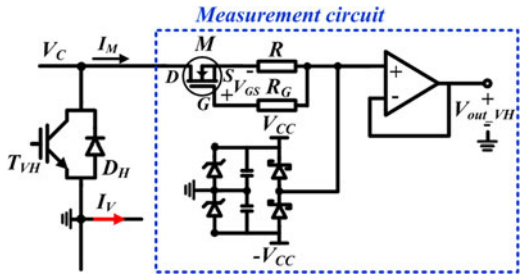

Fig. 3. Real-time $V_{\text{CE\_ON}}$ measurement circuit [15].

II. Preliminary Characterizations of an IGBT Module

Fig. 2 shows a configuration of a grid-connected inverter system based on two-level inverter, which is a typical circuit structure in various applications such as PV and wind-turbine systems [29]. The proposed method will be explained based on two-level grid-connected inverter. This section starts with the real-time $V_{\text{CE\_ON}}$ measurement circuit, which is used in this paper for the validation of the proposed method. Then, two kinds of preliminary *I–V* characterizations of the IGBT module are presented in order to separate the failure modes by using the $V_{\text{CE\_ON}}$ value measured at two points.

A. Real-Time $V_{\text{CE\_ON}}$ Measurement Circuit [15]

Fig. 3 shows the real-time $V_{\text{CE\_ON}}$ and V_F measurement circuit based on a depletion mode MOSFET (M) where the magnitude of clamping voltage (V_{CC}) should be larger than that of $V_{\text{CE\_ON}}$ and V_F. Considering T_{VH} as an example, when T_{VH} is turned on, the current I_{M} does not flow through M because the collector voltage $V_C = V_{\text{CE\_ON}} < V_{\text{CC}}$ and the input impedance of op-amp is high. Thus, $V_{\text{GS}} = 0$. Consequently, M is turned on since it has a negative threshold voltage ($V_T < V_{\text{GS}} = 0$), and thus, $V_{\text{out\_VH}} = V_{\text{CE\_ON}}$. When V_C increases above V_{CC} as T_{VH} is turned off, I_D starts to flow and makes a voltage drop in R. As I_M increases, V_{GS} becomes a negative value and then M is turned off when $V_{\text{GS}} < V_T$. Therefore, V_{CC} is measured at the output during this period.

It is worth mentioning that the proposed method is not specialized for this $V_{\text{CE\_ON}}$ measurement circuit. This method can be applied with other kinds of $V_{\text{CE\_ON}}$ measurement circuits.

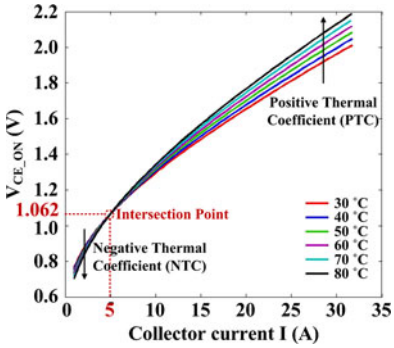

Fig. 4. Conventional *I–V* characterization of an IGBT.

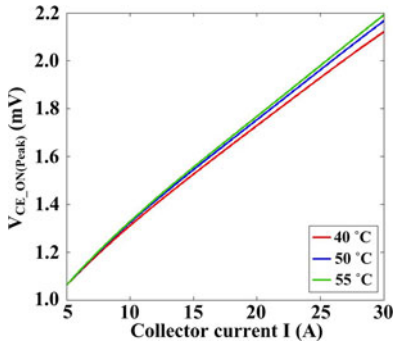

Fig. 5. *I–V* characterization of an IGBT using sinusoidal currents.

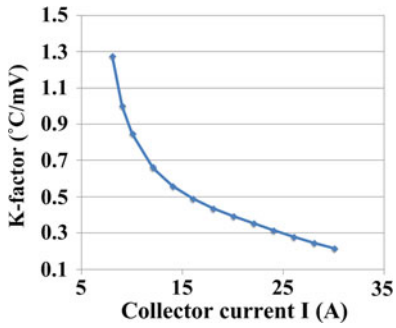

Fig. 6. *K*-factor from *I–V* characterization with sinusoidal currents.

B. Conventional I–V Characterization

The first one is a conventional *I–V* the characterization method by using a short current pulse under different temperatures, which is normally provided in datasheets of the IGBT modules. The data can be obtained by special equipment such as *V/I* curve tracer. It can also be obtained by using the configuration of an H-bridge converter with small-load inductors and an online V_{CE_ON} measurement circuit under particular switching sequences [16], [26].

Fig. 4 shows the conventional *I–V* characterization curves under different temperatures. From these curves, the intersection point between negative thermal coefficient (NTC) region and positive thermal coefficient (PTC) region, which is the first monitoring point of V_{CE_ON}, can be found. This point is independent of temperature, and thus, it can be used to determine the bond-wire fatigue, as proposed in [15] and [30].

C. I–V Characterization by Sinusoidal Currents

The other *I–V* characterization is by using sinusoidal currents in the operating range of the inverters under different temperatures, where V is V_{CE_ON} at peak current ($V_{CE\_ON(Peak)}$), I is the peak current and the temperature is the measurable temperature taken from outside of the IGBT module such as the heat-sink temperature (T_H), the case temperature (T_C), or the ambient temperature (T_A). In this paper, the heat-sink temperature is used for the *I–V* characterization. This characterization is performed under the assumption that the variation in T_H or T_C leads to the same variation in the junction temperature (T_j). Actually, this is not exactly the same, but experimental results in [16] have shown that 15 °C increase in T_H leads to 16.5 °C in T_j and the difference will be smaller as the output current decreases. However, this error is acceptable since a few degrees error is not significant to determine solder joint fatigue.

Fig. 5 shows the *I–V* characterization by using sinusoidal currents, and Fig. 6 shows a *K*-factor, which is the dependency of $V_{CE\_ON(Peak)}$ on T_j at a given current. Therefore, if the output current level of the inverter and heat-sink temperature are known, the reference V_{CE_ON} at the peak current ($V_{CE\_ON(Peak\_Ref)}$) can be obtained as (1), which is used for determining the failure mode described in Section III

$$V_{CE\_ON(Peak\_Ref)} = \frac{1}{K_{(I)}} \cdot (T_H - T_B) + V_{CE\_ON\_B(I)} \quad (1)$$

where $K_{(I)}$ is the *K*-factor as a function of current, T_H is the heat-sink temperature in real time, and $V_{CE\_ON\_B(I)}$ is the base V_{CE_ON} as a function of current, which can be chosen among the characterization curves. T_B is the base temperature corresponding to $V_{CE\_ON\_B(I)}$.

III. Failure Mode Separation Strategy Using V_{CE_ON} Measured at Two Points

In this section, the failure mode separation strategy by using V_{CE_ON} measured at two points is discussed by considering all possible cases. V_{CE_ON}s that are measured at the intersection point and measured at the peak current are remarked as $V_{CE\_ON(Int)}$ and $V_{CE\_ON(Peak)}$, respectively. From $V_{CE\_ON(Int)}$, the increased electrical resistance in the IGBT module due to bond-wire fatigue can be obtained. Then based on this value, the reference V_{CE_ON} at the peak current can be obtained from *I–V* characterization curves by sinusoidal current when the current level and reference temperature are known. Finally, by comparing the measured V_{CE_ON} at the peak current with the expected V_{CE_ON} at the peak current in real time, the failure mode in the IGBT module can be determined. The detailed explanation for each case is following.

A. Case 1: Bond-Wire Fatigue

Packaged devices do not permit to solely measure the V_{CE_ON} of devices. The measured V_{CE_ON} from the outside of an IGBT module definitely includes the voltage drop on various

interconnection elements. Therefore, it can be represented as

$$V_{\text{CE\_ON}} = V_{\text{CE\_ON(Chip)}} + R_{\text{eq}} \cdot I \tag{2}$$

where $V_{\text{CE\_ON(Chip)}}$ is the real on-state collector–emitter voltage of the device, R_{eq} is the equivalent resistance of the interconnection elements in the IGBT module, and I is the collector current.

The variation of R_{eq} ($\triangle R_{\text{eq}}$) due to bond-wire fatigue can be obtained by the increased value of $V_{\text{CE\_ON}}$ at the intersection point ($\triangle V_{\text{CE\_ON(Int)}}$) from the reference value ($V_{\text{CE\_ON(Int\_Ref)}}$), which can be obtained from the preliminary I–V characterization curves as shown in Fig. 3. Thus, $\triangle R_{\text{eq}}$ can be obtained as

$$\Delta V_{\text{CE\_ON(Int)}} = V_{\text{CE\_ON(Int)}} - V_{\text{CE\_ON(Int\_Ref)}} \tag{3}$$

$$\Delta R_{\text{eq}} = \frac{\Delta V_{\text{CE\_ON(Int)}}}{I_{\text{Int}}} \tag{4}$$

where $V_{\text{CE\_ON(Int)}}$ is the currently measured $V_{\text{CE\_ON}}$ at the intersection point and I_{Int} is the collector current at the intersection point.

From the obtained $\triangle R_{\text{eq}}$, the increment in $V_{\text{CE\_ON}}$ at the peak of output current due to bond-wire fatigue can be expected to be as

$$\Delta V_{\text{CE\_ON(Peak\_Ref)}} = \Delta R_{\text{eq}} \cdot I_{\text{Peak}} \tag{5}$$

where $\triangle V_{\text{CE\_ON(Peak\_Ref)}}$ is the increment in the $V_{\text{CE\_ON(Peak)}}$ from the initial I–V characterization by using sinusoidal currents and I_{Peak} is the peak of the output current.

From (5), the expected value of $V_{\text{CE\_ON}}$ under bond-wire fatigue can be obtained as

$$V_{\text{CE\_ON(Peak\_Exp)}} = V_{\text{CE\_ON(Peak\_Ref)}} + \Delta V_{\text{CE\_ON(Peak\_Ref)}} \tag{6}$$

where $V_{\text{CE\_ON(Peak\_Exp)}}$ is the expected $V_{\text{CE\_ON}}$ at the peak current and $V_{\text{CE\_ON(Peak\_Ref)}}$ is the reference $V_{\text{CE\_ON}}$ at the peak current from the initial I–V characterization by using sinusoidal currents.

If the there is a variation in R_{eq} and the $V_{\text{CE\_ON(Peak)}}$ is the same with $V_{\text{CE\_ON(Peak\_Exp)}}$ as given in (7), it can be expected that bond-wire fatigue occurs

$$\Delta R_{\text{eq}} > 0,\ V_{\text{CE\_ON(Peak)}} = V_{\text{CE\_ON(Peak\_Exp)}}. \tag{7}$$

B. Case 2: Solder Joint Fatigue

As mentioned in Section I, $V_{\text{CE\_ON(Peak)}}$ is varied when solder joint fatigue occurs. On the other hand, there is no variation in the $V_{\text{CE\_ON(Int)}}$ since it is independent on the temperature change. From the initial I–V characterization curves using sinusoidal currents as described in Section II, $V_{\text{CE\_ON(Peak\_Ref)}}$ can be obtained when the maximum current level (I_{Peak}) and heat-sink temperature (T_H) are known. If $V_{\text{CE\_ON(Peak)}}$ is higher than $V_{\text{CE\_ON(Peak\_Exp)}}$ and there is no variation in R_{eq} as given in (8), it can be expected that solder joint fatigue occurs

$$\Delta R_{\text{eq}} = 0, \qquad V_{\text{CE\_ON(Peak)}} > V_{\text{CE\_ON(Peak\_Exp)}}. \tag{8}$$

Further, the increment in T_j due to solder joint fatigue can be obtained indirectly by the K-factor and the difference between $V_{\text{CE\_ON(Peak)}}$ and $V_{\text{CE\_ON(Peak\_Exp)}}$.

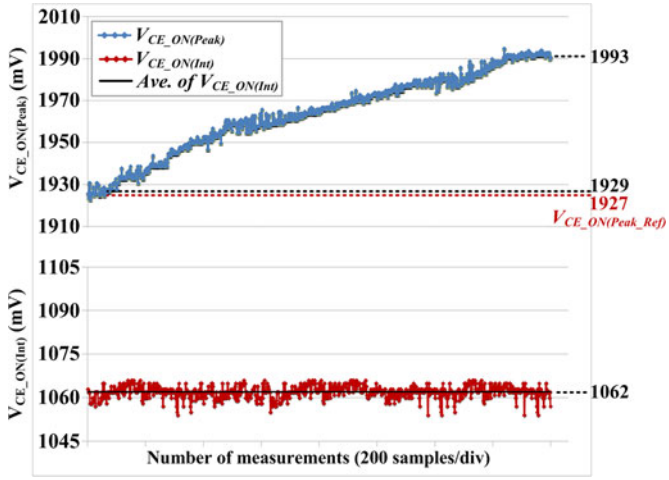

Fig. 7. Experimental result under virtual solder joint fatigue when $I = 25\ \text{A}_{\text{peak}}$ (Case 2).

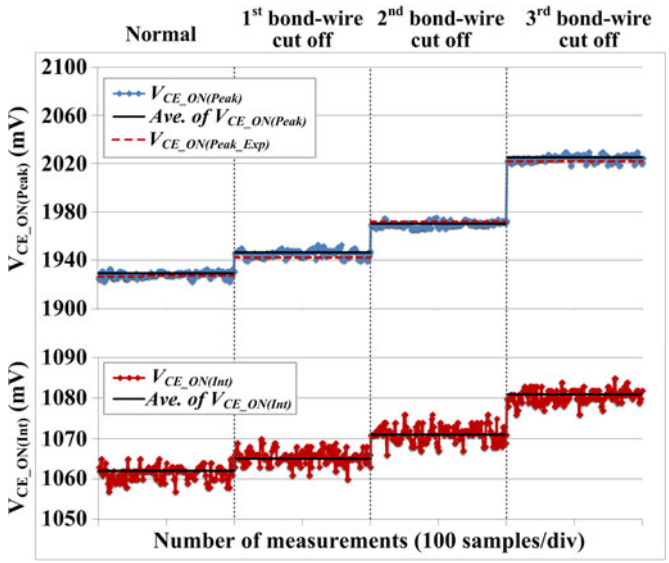

Fig. 8. Experimental result under bond-wire fatigue when $I = 25\ \text{A}_{\text{peak}}$ (Case 1).

C. Case 3: Bond-Wire and Solder Joint Fatigues

Under the both failure modes, bond-wire fatigue leads to an increase of R_{eq} and solder joint fatigue will make $V_{\text{CE\_ON(Peak)}}$ larger than $V_{\text{CE\_ON(Peak\_Exp)}}$. Thus, it can be expected that both failure modes occur if condition (9) is satisfied

$$\Delta R_{\text{eq}} > 0, \qquad V_{\text{CE\_ON(Peak)}} > V_{\text{CE\_ON(Peak\_Exp)}}. \tag{9}$$

Further, the contribution of each failure mode on the $V_{\text{CE\_ON(Peak)}}$ increase from the $V_{\text{CE\_ON(Peak\_Ref)}}$ can be separated.

IV. Experimental Results

Experiments have been carried out in order to confirm the validity of the proposed strategy. A three-phase IGBT module is used in this paper, and T_{VL}, as shown in Fig. 2, is the target device in the experiments. Bond-wire fatigue is simulated by cutting the bond-wires of an open IGBT module. In the case of solder joint fatigue, virtual solder joint fatigue is emulated by

TABLE I
VARIATION OF MONITORING PARAMETERS UNDER BOND-WIRE FATIGUE WHEN $I = 25\,A_{peak}$ (CASE 1)

	$V_{CE\_ON(Int)}$	$\triangle V_{CE\_ON(Int)}$	$\triangle R_{eq}$	$V_{CE\_ON(Peak)}$	$V_{CE\_ON(Peak\_Exp)}$	Error
Normal	1062 mV	–	–	1929 mV	1927 mV	+2 mV
First bond-wire cutoff	1065 mV	3 mV	0.6 mΩ	1946 mV	1942 mV	+4 mV
Second bond-wire cutoff	1071 mV	9 mV	1.8 mΩ	1970 mV	1972 mV	−2 mV
Third bond-wire cutoff	1081 mV	19 mV	3.8 mΩ	2025 mV	2022 mV	+3 mV

changing T_H using an external heater system. This way is not totally the same with the real solder joint fatigue, but it can emulate the increase of T_j due to solder joint fatigue reasonably in order to validate the proposed method. The on-state collector–emitter voltage (V_{CE_ON}) is measured by the measurement circuit proposed in [15]. $V_{CE\_ON(Int)}$ and I_{Int} are obtained from the preliminary characterizations (see Fig. 2) and they are 1.062 V and 5 A, respectively. Further, the average of 100 V_{CE_ON} measurements at both intersection and peak current points are used in order to improve the accuracy.

Fig. 7 shows the experimental result, which is simulating Case 2 in Section III under the following condition: $V_{DC} = 350\,V$, $I = 25\,A_{peak}$, $V_{out} = 163\,V$, modulation index $= 0.806$, $f_{sw} = 10\,kHz$, $f_{out} = 50\,Hz$, and $T_H = 40\,^{\circ}C$. The measured $V_{CE\_ON(Int)}$ is the same as the value from the preliminary I–V characterization, and it is 1062 mV. Under the given condition, $V_{CE\_ON(Peak\_Ref)}$ can be obtained as 1929 mV based on (1). The measured $V_{CE\_ON(Peak)}$ is 1927 mV, which is almost the same as $V_{CE\_ON(Peak\_Ref)}$. There is no change in $V_{CE\_ON(Int)}$ and $V_{CE\_ON(Peak)}$ is almost the same as the $V_{CE\_ON(Peak\_Ref)}$, and thus, it can be expected that the IGBT module is under the normal condition. Then, T_H increases from 40 to 60 °C in order to simulate a virtual solder joint fatigue. It can be seen that there is no variation in $V_{CE\_ON(Int)}$, and therefore, $\triangle R_{eq} = 0$. On the other hand, $V_{CE\_ON(Peak)}$ increases from 1927 to 1993 mV. $V_{CE\_ON(Peak)}$ is 64 mV larger than $V_{CE\_ON(Peak\_Ref)}$. This result satisfies (8), which is the condition for determining solder joint fatigue. Further, from the difference between $V_{CE\_ON(Peak)}$ and $V_{CE\_ON(Peak\_Ref)}$ and K-factor at 25 A, the increment in T_j can be obtained indirectly, which is 19.2 °C [64 mV · 0.3 (°C/mV)]. This result agrees well with the variation of T_H, and thus, T_j increase due to real solder joint fatigue can be determined.

Fig. 8 shows the experimental result, where Case 1 is emulated. Three bond-wires are cut among five bond-wires in consecutive order and the related values of the monitoring parameters are summarized in Table I. For example, when three bond-wires are cut off, $V_{CE\_ON(Int)}$ increases from 1062 to 1081 mV. Therefore, $\triangle R_{eq}$ is 3.8 mΩ (19 mV/5 A). From this, it can be expected that $V_{CE\_ON(Peak)}$ will increase by 95 mV from $V_{CE\_ON(Peak\_Ref)} = 1927\,mV$ due to bond-wire fatigue, and consequently, $V_{CE\_ON(Peak\_Exp)}$ is 2022 mV. $V_{CE\_ON(Peak)}$ is measured as 2025 mV after cutting off three bond-wires, and it is almost the same with $V_{CE\_ON(Peak\_Exp)}$. In conclusion, there is an increase in R_{eq} and $V_{CE\_ON(Peak)}$ is the same with $V_{CE\_ON(Peak\_Exp)}$. This result corresponds to (7) for indicating bond-wire fatigue. It can also be seen that the other cases in Table I also meet the condition given in (7).

Fig. 9 shows the experiment result under both failure modes. First, bond-wire fatigue is simulated by cutting two bond-wires among five bond-wires. $V_{CE\_ON(Int)}$ increases by 9 mV, and thus, $\triangle R_{int}$ is 1.8 mΩ. From this, $\triangle V_{CE\_ON(Peak\_Ref)}$ is obtained as 45 mV as in (5), and finally, $V_{CE\_ON(Peak\_Exp)}$ can be obtained as 1972 mV. After cutting off two bond-wires, $V_{CE\_ON(Peak)}$ rises by 44 mV from 1929 to 1973 mV, which is almost the same with $V_{CE\_ON(Peak\_Exp)}$. Then, T_H is changed from 40 to 49 °C in order to emulate virtual solder joint fatigue at the same time. $V_{CE\_ON(Int)}$ is kept to 1071 mV, which is increased by bond-wire fatigue.

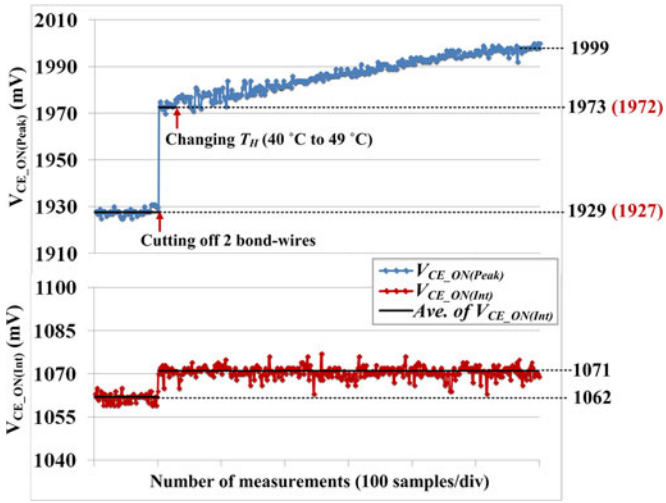

Fig. 9. Experimental result under both bond-wire and virtual solder joint fatigue when $I = 25\,A_{peak}$ (Case 3).

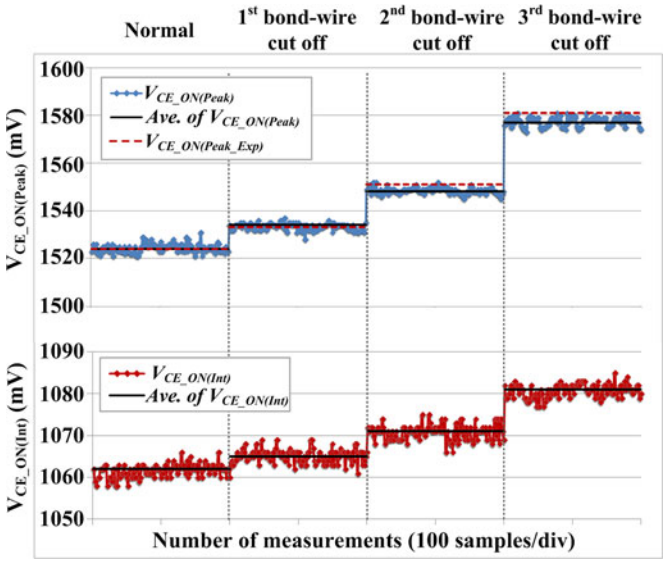

Fig. 10. Experimental result under bond-wire fatigue when $I = 15\,A_{peak}$ (Case 1).

TABLE II
VARIATION OF MONITORING PARAMETERS UNDER BOND-WIRE FATIGUE WHEN $I = 15\,A_{peak}$ (CASE 1)

	$V_{CE\_ON(Int)}$	$\triangle V_{CE\_ON(Int)}$	$\triangle R_{eq}$	$V_{CE\_ON(Peak)}$	$V_{CE\_ON(Peak\_Exp)}$	Error
Normal	1062 mV	–	–	1524 mV	1524 mV	0 mV
First bond-wire cutoff	1065 mV	3 mV	0.6 mΩ	1534 mV	1533 mV	+1 mV
Second bond-wire cutoff	1071 mV	9 mV	1.8 mΩ	1548 mV	1551 mV	−3 mV
Third bond-wire cutoff	1081 mV	19 mV	3.8 mΩ	1577 mV	1581 mV	−4 mV

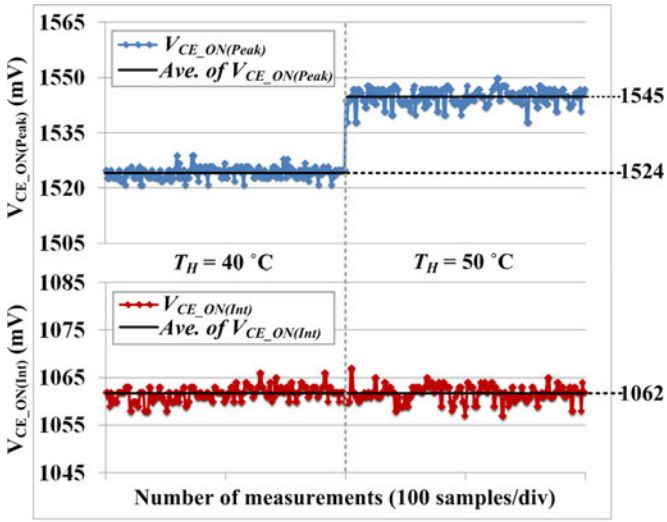

Fig. 11. Experimental result under virtual solder joint fatigue when $I = 15\,A_{peak}$ (Case 2).

On the other hand, $V_{CE\_ON(Peak)}$ increases from 1973 to 1999 mV. $V_{CE\_ON(Peak)}$ is 26 mV larger than $V_{CE\_ON(Peak\_Exp)}$, which means that there is about 8 °C increase in T_j due to solder joint fatigue. Compared with the initial value, $V_{CE\_ON(Peak)}$ increases by 70 mV, and it is possible to determine that the 44 mV increase is due to bond-wire fatigue and the 26 mV increase is caused by solder joint fatigue. This result is in agreement with (9). Further, in the case of solder joint fatigue, the amount of T_j increase can be obtained indirectly.

The proposed method is also validated under another output current considering Case 1 and Case 2.

Fig. 10 shows the experimental result under bond-wire fatigue when the output current is 15 A_{peak}. The obtained values are summarized in Table II. It can be seen that the same $\triangle R_{eq}$ is obtained with $\triangle R_{eq}$ when $I = 25\,A_{peak}$. Further, under all cases, $V_{CE\_ON(Peak)}$ is almost the same with $V_{CE\_ON(Peak\_Exp)}$ within 4 mV error.

In addition, virtual solder joint fatigue is simulated by changing T_H from 40 to 50 °C. As shown in Fig. 11, there is no variation in $V_{CE\_ON(Int)}$ but $V_{CE\_ON(Peak)}$ increases by 21 mV, which means a 11 °C rise (21 mV · 0.53 (°C/mV) in T_j.

It can be seen that both experimental results meet conditions (7) and (8) for determining each failure mode, respectively.

V. CONCLUSION

In this paper, a method for separation of wear-out failure modes of IGBT modules has been proposed. The proposed method can be achieved by monitoring V_{CE_ON} at intersection point of *I–V* characterization curves and the peak of output currents. By the proposed method, the wear-out condition of IGBT modules in grid-connected inverters can be monitored in real time with the determination of failure modes.

The proposed method does not need re-characterizations of *I–V* curves of the component as it is worn-out. This method just needs two preliminary *I–V* characterizations of the IGBT module that are the conventional *I–V* characterization and the *I–V* characterization using sinusoidal current in the operating range of the inverter under the different reference temperature, which is measurable from outside of the IGBT module such as heat-sink temperature (T_H), case temperature (T_C) or ambient temperature (T_A). Therefore, this method is convenient and very suitable for real converter applications. In addition, the proposed method can also be applied not only to grid-connected inverter with fixed modulation index but also to other applications such as motor drives systems with defined mission profiles and other inverters with variable dc-link voltage even though it requires more effort on the *I–V* characterization by sinusoidal currents.

The validity of the proposed method has been confirmed by the experiments with the open IGBT module where bond-wire fatigue and solder joint fatigue are simulated by cutting bond-wires and changing the heat-sink temperature, respectively.

The proposed method allows proactive maintenance plans by monitoring the wear-out condition of an IGBT module in real-time. Further, it is also expected to improve the reliability and availability of power electronic systems by helping to apply proactive control strategies depending on the different wear-out failure modes for extending the lifetime of the inverter.

REFERENCE

[1] H. Wang, M. Liserre, and F. Blaabjerg, "Toward reliable power electronics: Challenges, design tools, and opportunities," *IEEE Ind. Electron. Mag.*, vol. 7, no. 2, pp. 17–26, Jun. 2013.
[2] L. M. Moore and H. N. Post, "Five years of operating experience at a large, utility-scale photovoltaic generating plant," *Progress Photovoltaic: Res. Appl.*, vol. 16, no. 3, pp. 249–259, 2008.
[3] Reliawind, Project Final Report on Reliability Focused Research on Optimizing Wind Energy Systems Design, Operation and Maintenance: Tools, Proof of Concepts, Guidelines & Methodologies for a New Generation, 2011. [Online]. Available: http://cordis.europa.eu/publication/rcn/14854_en.html
[4] H. Wang *et al.*, "Transitioning to physics-of-failure as a reliability driver in power electronics," *IEEE J. Emerging Sel. Topics Power Electron.*, vol. 2, no. 1, pp. 97–114. Mar. 2014.
[5] S. Yang, A. Bryant, P. Mawby, D. Xiang, L. Ran, and P. Tavner, "An industry-based survey of reliability in power electronic converters," *IEEE Trans. Ind. Appl.*, vol. 47, no. 3, pp. 1441–1451, May /Jun. 2011.
[6] U. M. Choi, F. Blaabjerg, and K. B. Lee, "Study and handling methods of power IGBT module failures in power electronic converter systems," *IEEE Trans. Power Electron.*, vol. 30, no. 5, pp. 2517–2533. May 2015.
[7] A. Volke and M. Hornkamp, IGBT Modules - Technologies, Driver and Application, Infineon Technologies AG, Munich, 2011. ISBN: 978-3-00-032076-7.

[8] K. Ma and F. Blaabjerg, "The impact of power switching devices on the thermal performance of a 10 MW wind power NPC converter," *Energies*, vol. 5, no. 7, pp. 2559–2577, Jul. 2012.
[9] C. Busca *et al.*, "An overview of the reliability prediction related aspects of high power IGBTs in wind power applications," *Microelectron. Rel.*, vol. 51, no. 9-11, pp. 1903–1907, Sep. -Nov. 2011.
[10] M. Ciappa, "Selected failure mechanism of modern power modules," *Microelectron. Rel.*, vol. 42, no. 4-5, pp. 653–667, Apr.–May 2002.
[11] U. M. Choi, F. Blaabjerg, and S. Jorgensen, "Power cycling test methods for reliability assessment of power device modules in respect to temperature stress," *IEEE Trans. Power Electron.*, accepted, early access article, 2017. DOI: 10.1109/TPEL.2017.2690500.
[12] Y. Avenas, L. Dupont, and Z. Khatir, "Temperature measurement of power semiconductor devices by thermo-sensitive electrical parameters—A review," *IEEE Trans. Power Electron.*, vol. 27, no. 6, pp. 3081–3092. Jun. 2012.
[13] U. Scheuermann and R. Schmidt, "Impact of solder fatigue on module lifetime in power cycling tests," in *Proc. EPE'11 ECCE-Eur.*, Aug. 2011, pp. 1–10.
[14] V. Smet, F. Forest, J. J. Huselstein, A. Rashed, and F. Richardeau, "Evaluation of vce monitoring as a real-time method to estimate aging of bond-wire IGBT modules stressed by power cycling," *IEEE Trans. Ind. Electron.*, vol. 60, no. 7, pp. 2760–2770, Jul. 2013.
[15] U. M. Choi, F. Blaabjerg, S. Munk-Nielsen, S. Jorgensen, and B. Rannestad, "Reliability improvement of power converters by means of condition monitoring of IGBT modules," *IEEE Trans. Power Electron.*, vol. 32, no. 10, pp. 7990–7997, Oct. 2017.
[16] U. M. Choi, F. Blaabjerg, F. Iannuzzo, and S. Jørgensen, "Junction temperature estimation method for a 600 V, 30A IGBT module during converter operation," *Microelectron. Rel.*, vol. 55, no. 9–10, pp. 2022–2026, Aug.–Sep. 2015.
[17] B. Ji, "In-situ health monitoring of IGBT power modules in EV applications," Ph.D. dissertation, School of Elect. Electron. Eng., Newcastle University, Newcastle, U.K., Dec. 2011.
[18] U. M. Choi, F. Blaabjerg, and K. B. Lee, "Reliability improvement of a T-Type three-level inverter with fault-tolerant control strategy," *IEEE Trans. Power Electron.*, vol. 30, no. 5, pp. 2660–2673, May 2014.
[19] B. Welchko, T. Lipo, T. Jahns, and S. Schulz, "Fault-tolerant three-phase AC motor drive topologies: A comparison of features, cost, and limitations," *IEEE Trans. Power Electron.*, vol. 60, no. 8, pp. 3360–3371, Jul. 2004.
[20] M. Naidu, S. Gopalakrishnam, and T. Nehl, "Fault-tolerant permanent magnet motor drive topologies for automotive X-By-wire systems," *IEEE Trans. Ind. Appl.*, vol. 46, no. 2, pp. 841–848, Mar.–Apr. 2010.
[21] W. Zhang, D. Xu, P. N. Enjeti, H. Li, J. T. Hawke, and H. S. Krishnamoorthy, "Survey on fault-tolerant techniques for power electronic converters," *IEEE Trans. Power Electron.*, vol. 29, no. 12, pp. 6319–6331, Dec. 2014.
[22] Y. Yang, H. Wang, F. Blaabjerg, and T. Kerekes, "A hybrid power control concept for PV inverters with reduced thermal loading," *IEEE Trans. Power Electron.*, vol. 29, no. 12, pp. 6171–6275. Dec. 2014.
[23] K. Ma and F. Blaabjerg, "Modulation methods for three-level neutral-point-clamped inverter achieving stress redistribution under moderate modulation index," *IEEE Trans. Power Electron.*, vol. 31, no. 1, pp. 5–10, Jan. 2016.
[24] P. Ghimire, I. Trintis, S. Munk-Nielsen, and B. Rannestad, "Ageing monitoring in IGBT module under sinusoidal loading," *Microelectron. Rel.*, vol. 55, no. 9–10, pp. 1945–1949, Aug.–Sep. 2015.
[25] I. Vernica, K. Ma, and F. Blaabjerg, "Advanced derating strategy for extended lifetime of power electronics in wind power applications," in *Proc. PEDG*, Jun. 2016, pp. 1–8.
[26] U. M. Choi, S. Jørgensen, and F. Blaabjerg, "Advanced accelerated power cycling test for reliability investigation of power device modules," *IEEE Trans. Power Electron.*, vol. 31, no. 12, pp. 8371–8386, Dec. 2016.
[27] N. Baker, S. Munk-Nielsen, F. Iannuzzo, and M. Liserre, "IGBT junction temperature measurement via peak gate current," *IEEE Trans. Power Electron.*, vol. 31, no. 5, pp. 3784–3793, May 2015.
[28] H. Luo, Y. Chen, P. Sun, W. Li, and X. He, "Junction temperature extraction approach with turn-off delay time for high-voltage high-power IGBT modules," *IEEE Trans. Power Electron.*, vol. 31, no. 7, pp. 5122–5132, Jul. 2016.
[29] E. Romero-Cadaval, G. Spagnuolo, L. G. Franquelo, C. A. Ramos-Paja, T. Suntio, and W. M. Xiao, "Grid-connected photovoltaic generation plants: Components and operation," *IEEE Ind. Electron. Mag.*, vol. 7, no. 3, pp. 6–20, Sep. 2013.
[30] A. Singh, A. Anurag, and S. Anand, "Evaluation of Vce at inflection point for monitoring bond wire degradation in discrete packaged IGBTs," *IEEE Trans. Power Electron.*, vol. 32, no. 4, pp. 2481–2484, Apr. 2017.

Ui-Min Choi (S'11–M'16) received the B.S. and M.S. degree from Ajou University, Suwon, Korea, in 2011 and 2013, respectively, and the Ph.D. degree from Aalborg University, Aalborg, Denmark, in 2016, all in electrical engineering.

He is currently Post-Doctoral Researcher with the Department of Energy Technology, Aalborg University. His current research interests include reliability of power device and power converter systems, renewable energy generation, and multilevel converter.

Dr. Choi received the IEEE Transactions on Power Electronic Second Prize Paper Award in 2017.

Frede Blaabjerg (S'86–M'88–SM'97–F'03) received the Ph.D. degree in electrical engineering from Aalborg University, Aalborg, Denmark, in 1992.

He was with ABB-Scandia, Randers, from 1987 to 1988. He became an Assistant Professor in 1992, an Associate Professor in 1996, and a Full Professor in power electronics and drives in 1998 at Aalborg University. He has been a part-time Research Leader at Research Center Risoe. From 2006 to 2010, he was the Dean of the Faculty of Engineering, Science, and Medicine and became a Visiting Professor at Zhejiang University, China, in 2009. His current research interests include power electronics and its applications such as in wind turbines, PV systems, reliability, harmonics, and adjustable speed drives.

Dr. Blaabjerg was an Editor-in-Chief of the IEEE TRANSACTIONS ON POWER ELECTRONICS 2006–2012. He was a Distinguished lecturer for the IEEE Power Electronics Society 2005–2007 and for the IEEE Industry Applications Society from 2010 to 2011. He has been the Chairman of EPE in 2007 and PEDG, Aalborg, in 2012. He received the 1995 Angelos Award for his contribution in modulation technique and the Annual Teacher prize at Aalborg University. In 1998, he received the Outstanding Young Power Electronics Engineer Award from the IEEE Power Electronics Society. He has received 15 IEEE Prize paper awards and another prize paper award at PELINCEC Poland 2005. He received the IEEE PELS Distinguished Service Award in 2009 and the EPE-PEMC 2010 Council Award and the IEEE William E. Newell Power Electronics Award 2014. He has received a number of major research awards in Denmark.